Chemical Engineering Science 104 (2013) 201–207

Contents lists available at ScienceDirect

Chemical Engineering Science

journal homepage: www.elsevier.com/locate/ces

Detailed numerical simulation of an intruder impacting on a granular bed using a hybrid discrete particle and immersed boundary (DP-IB) method

Y. Xu [a], J.T. Padding [a,*], M.A. van der Hoef [b], J.A.M. Kuipers [a]

[a] Department of Chemical Engineering and Chemistry, Eindhoven University of Technology, 5600 MB Eindhoven, The Netherlands
[b] Department of Science and Technology, University of Twente, 7500 AE Enschede, The Netherlands

HIGHLIGHTS

- A simulation method for an intruder moving through a bed of particles is introduced.
- An unresolved discrete particle method is used for the granular particles.
- A resolved immersed boundary method is used for the intruder.
- Force on intruder impacting on a prefluidized bed is in agreement with experiments.
- The direct effect of interstitial gas is quantified for Geldart-B granular particles.

GRAPHICAL ABSTRACT

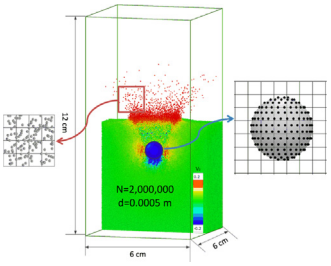

ARTICLE INFO

Article history:
Received 11 May 2013
Received in revised form
25 July 2013
Accepted 2 September 2013
Available online 17 September 2013

Keywords:
Fluidized granular bed
Impact cratering
Moving internals
Gas-induced force
Immersed boundary method

ABSTRACT

We numerically study the impact of a large sphere dropping into a prefluidized granular bed using a state-of-the-art hybrid discrete particle and immersed boundary (DP-IB) method. For the first time, both the gas-induced drag force and the contact force exerted on the intruder are investigated separately. Our results show that even for relatively large granular particles of 0.5 mm diameter, namely Geldart B particles, and an intruder of 1 cm, the drag exerted by the interstitial gas accounts for up to 5% of the total force experienced by the intruder. Our simulation results match well with existing experimental observations. This work shows that the current simulation scheme could become a tool to investigate the effect of interstitial gas on the dynamics of projectile impact cratering. More generally, the method allows for accurate simulation of the hydrodynamic effects of large internal objects moving through (pre-)fluidized granular beds.

1. Introduction

Studies of forces resisting a big intruder moving through a granular medium can help us understand phenomena such as footprints on sand and the craters of the lunar surface. When an intruder moves through a granular bed, the force on the intruder shows complex behaviour caused by the inhomogeneity of the force propagation and the requirement for grain reorganization. Phenomenological models have been proposed to account for experimental results of the force on a vertically falling object impacting onto a horizontal bed of granular particles. Uehara et al. (2003) showed that the absolute final penetration depth, d, is a power of the total drop distance, $H=h+d$, where h is the free-fall distance, which could be interpreted in terms of a stopping force that

* Corresponding author. Tel.: +31 402473674; fax: +31 402475833.
E-mail address: j.t.padding@tue.nl (J.T. Padding).

0009-2509/$ - see front matter © 2013 Elsevier Ltd. All rights reserved.
http://dx.doi.org/10.1016/j.ces.2013.09.023

is a product of powers of depth and speed. Walsh and de Bruyn (2004) showed that the penetration depth, d, scales linearly with the speed at impact, $v_0 = -(2gh)^{1/2}$ with g=980 cm s^{-2}, corresponding to a force that is linear in speed. Pica Ciamarra et al. (2004) showed that the stopping time, t_{stop}, seems constant for fast impacts, which was interpreted by a force that is constant during the cratering process but proportional to the initial impact speed. Lohse et al. (2004) showed that depth versus time is a sinusoid in the limit of a zero-speed impact, which was interpreted by a force that is equal to gravity, mg, plus a Coulomb friction term proportional to depth. Later, Katsuragi and Durian (2007) studied the granular impact cratering process with high resolution equipment. In their experiments, spherical glass beads (diameter range 250–350 μm, density $\rho_g = 1.52$ g cm^{-3} and friction coefficient $\mu = 0.45$) were used as granular medium. The medium was fluidized, and gradually defluidized by a uniform upflow of N_2 gas. The volume fraction occupied by the beads was 0.590 ± 0.004 after fluidization. A steel sphere of diameter $D_b = 2.54$ cm was used as a projectile. One single force law was proposed and with this force model, results in Uehara et al. (2003), Walsh and de Bruyn (2004), Pica Ciamarra et al. (2004), and Lohse et al. (2004) could be interpreted.

However, Durian and co-workers derived a different functional form for the force model based on their shallow impact catering experiments (Ambroso et al., 2005a). In their experiments, similar glass beads of diameter $D_g = 0.30 \pm 0.05$ mm were prepared at 59% packing fraction also by slowly turning off a fluidizing upflow of air. Intruders made from different material and different diameters were employed.

Goldman and Umbanhowar (2008) used direct measurements of the forces exerted on a sphere during the penetration of a granular medium from which a new force law was proposed. In their experiments, two jumps of the force during impact were found: a rapid, velocity-dependent increase upon the initial contact and a similarly sharp depth-dependent decrease as the impacting object comes to rest.

To gain detailed force profiles, these experiments (Katsuragi and Durian, 2007; Ambroso et al., 2005a; Goldman and Umbanhowar, 2008) were usually done by attaching a thread or a rod to the intruder, with some finely striped graduation carved on them. Then the speed and the acceleration were deduced from the displacement of the striped pattern between successive frames shot by a high speed camera. Because of the resolution of the devices, different force profiles were obtained in different experiments (Katsuragi and Durian, 2007; Ambroso et al., 2005a; Goldman and Umbanhowar, 2008) and then different force laws were deduced.

Clearly, the form of the force experienced by an impacting intruder is still not unified, and understanding of this problem remains limited. At the same time, new questions arise, such as what the relative role is of the gas phase.

For relatively large (Geldart B type) granular particles, it is argued in Ambroso et al. (2005b) that the effect of gas on the intruder penetration depth is negligible. It may be argued on dimensional grounds that the interstitial gas must play an increasingly important role as the size of the granular particles decreases: the mass of a granular particle scales with a higher power of its diameter than the drag force it experiences when moving relative to the surrounding gas. Unfortunately, until now it was not possible to measure the gas-induced force on the intruder separately experimentally. In recent years, some researchers have attempted to study this problem using discrete element method (DEM) (Wang et al., 2012; Pica Ciamarra et al., 2004; Kondic et al., 2012; Wada et al., 2006). Although some new results have been shown, the precise effect of the gas on the dynamics of an intruder in a packed bed of Geldart B particles still remains unclear.

For smaller (Geldart A type) particles, after the pioneering work by Thoroddsen and Shen (2001) showed the formation of granular jets, a lot of fruitful work (Caballero et al., 2007; Royer et al., 2011, 2007, 2008) has been done to investigate the role of gas. These studies focus on global effects of the granular motion such as collapse of gas voids and the formation of granular eruptions; they do not quantitatively measure the gas-induced force on the intruder. The granular particles in these studies are fine powders with a particle diameter of up to 100 μm, which are generally very non-spherical and rough (often angular fine sand particles). Partly because of the non-spherical shape, after pre-fluidization these powders form very loose beds with a low solid volume fraction of less than 0.5 and often include trapped air bubbles. Such beds are extremely susceptible to gas flows induced by an intruder, and consequently show spectacular phenomena such as uprising particle jets. Even smaller (Geldart C type) particles, with a mean diameter of less than 30 μm, are usually cohesive particles. Such particles are extremely difficult to fluidize because the interparticle attractive Van der Waals forces are relatively large.

In this paper we introduce a state-of-the-art discrete particle method (DPM) combined with an immersed boundary (IB) method to investigate the kinematics of an intruder dropping onto a prefluidized granular bed. We apply our method to the case of relatively large spherical Geldart B type granular particles for two reasons: (1) because the contact model for such particles is well defined and accurate and (2) because for such systems accurate experiments are available (Ambroso et al., 2005a) for validation. We will show that, overall, our simulation results are in good agreement with these experimental observations. For the particular size of the granular particles (0.5 mm diameter) and intruder (1 cm diameter) shown here, we find that the direct gas drag on the intruder is relatively small, but not negligible, up to 5% of the total force on the intruder. Simulation without any gas confirms that there is also an indirect effect of the gas on the kinematics of the granular particles.

Our work shows that the current simulation scheme could become a powerful tool to investigate the effect of interstitial gas on the dynamics of projectile impact cratering. In this respect it is important to note that there is no fundamental reason why our method cannot be applied to smaller Geldart A type particles as well, but this would first require another extensive study on accurate contact models for rough and non-spherical particles leading to the stable and relatively loose packings studied in Caballero et al. (2007), Royer et al. (2011), and Royer et al. (2007, 2008). Similar arguments apply to the even smaller Geldart C type particles, with respect to accurate models for the cohesive forces. More generally, the method allows for accurate simulation of the hydrodynamic effects of large objects of any shape – such as stirrers, baffles and other internals – in (pre-)fluidized granular beds.

2. Model description

Our model consists of two major sub-models, the discrete particle (DP) and immersed boundary (IB) models. The DP model deals with the motion of suspended small (granular) particles, taking into account the action of gravity, gas–solid drag forces, as well as particle–particle and particle–wall collisions. In this model, the gas phase is solved on a computational mesh with a length scale larger than the size of the small particles and the gas–particle coupling is treated by empirical drag relations (Van der Hoef et al., 2006). The IB method deals with the motion of the big intruder through the continuous phase (consisting of gas and suspended solid particles). We now give a brief technical description of the DP model and the IB method. A schematic representation of the DP model and the IB method is shown in Fig. 1.

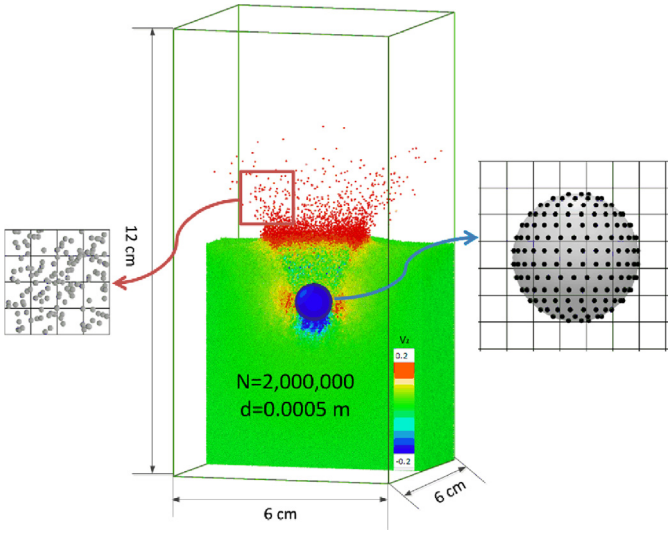

Fig. 1. Schematic representation of the DP and IB methods. In the DP model the motion of the suspended small particles is solved, taking into account detailed solid–solid contact forces, as well as drag forces caused by motion relative to the interstitial gas phase. The particles are smaller than the grid on which the gas phase equations are solved (left), requiring the use of empirical drag relations. On the contrary, the intruder is much larger than the gas grid. Coupling between the intruder and the gas phase is accomplished through the IB method, which enforces no-slip boundary conditions by homogenous distribution of force points across the surface of the intruder (right). Schematic representation of the bed geometry is also shown in this figure, prior to dropping the large intruder, the granular bed is fluidized and slowly de-fluidized. Only half of the bed is shown and the particles are colour coded according to the velocity in the z-direction. Visualization was carried out using OVITO (Stukowski, 2009). (For interpretation of the references to colour in this figure caption, the reader is referred to the web version of this article.)

2.1. Equations of motion for the small particles

The translational and rotational motion of a particle a with mass m_a, moment of inertia I_a and coordinate $\mathbf{r}_a$ can be described by Newton's equations for rigid body motion:

$$m_a\frac{\mathrm{d}^2\mathbf{r}_a}{\mathrm{d}t^2}=\mathbf{F}_{\mathrm{g},a}+\mathbf{F}_{\mathrm{d},a}+\mathbf{F}_{\mathrm{p},a}+\mathbf{F}_{\mathrm{c},a}, \tag{1}$$

$$I_a\frac{\mathrm{d}\boldsymbol{\omega}_a}{\mathrm{d}t}=\mathbf{T}_a, \tag{2}$$

The four terms on the right-hand side of Eq. (1) account for the gravitational force, the gas drag force, the force due to pressure gradients in the gas phase, and the sum of the individual contact forces exerted by all other particles in contact with particle a. In Eq. (2), $\boldsymbol{\omega}_a$ is the angular velocity and $\mathbf{T}_a$ is the torque around the centre-of-mass of particle a. Regarding the contact model, two types of collision models are widely used, namely the hard sphere model and the soft sphere model. In our simulation, the soft sphere model is used since the hard sphere model is not suited for systems where quasi-static particle configurations exist, more detailed information can be found in Van der Hoef et al. (2006) and Alder and Wainwright (1957).

For the calculation of $\mathbf{F}_{\mathrm{contact},a}$, a three-dimensional 3D linear spring and a dashpot type soft sphere collision model along the lines of Cundall and Strack is used (Cundall and Strack, 1979; van Sint Annaland et al., 2005; Xiong et al., 2012). In this model, the total contact force on particle a of radius R_a is given by a sum of normal and tangential pair forces with neighbouring particles,

$$\mathbf{F}_{\mathrm{contact},a}=\sum_{b\,\in\,\mathrm{contact\ \ list}}(\mathbf{F}_{n,ab}+\mathbf{F}_{t,ab}) \tag{3}$$

where the normal forces $\mathbf{F}_{n,ab}$ depend linearly on the overlap $\delta=R_a+R_b-|\mathbf{r}_a-\mathbf{r}_b|$ and the relative normal velocity $\mathbf{v}_{n,ab}=((\mathbf{v}_a-\mathbf{v}_b)\cdot\mathbf{n}_{ab})\mathbf{n}_{ab}$, with $\mathbf{n}_{ab}$ being the unit vector pointing from the centre of b to the centre of a. Similarly, the tangential forces $\mathbf{F}_{t,ab}$ depend linearly on the tangential overlap $\boldsymbol{\delta}_t$, defined as the integral of the relative tangential velocity from the time of first contact, and the relative tangential velocity $\mathbf{v}_{t,ab}=(\mathbf{v}_a-\mathbf{v}_b)-\mathbf{v}_{n,ab}$ itself. The tangential forces also lead to a torque on the particles:

$$\mathbf{T}_a=\sum_{b\,\in\,\mathrm{contact\ \ list}}(R_a\mathbf{n}_{ab}\times\mathbf{F}_{t,ab}) \tag{4}$$

2.2. Governing equations for the gas phase

The gas flow is governed by the conservation equations for mass and momentum:

$$\frac{\partial(\varepsilon\rho_g)}{\partial t}+\nabla\cdot\varepsilon\rho_g\mathbf{u}=0 \tag{5}$$

$$\frac{\partial(\varepsilon\rho_g\mathbf{u})}{\partial t}+\nabla\cdot\varepsilon\rho_g\mathbf{u}\mathbf{u}=-\varepsilon\nabla p-\nabla\cdot\varepsilon\boldsymbol{\tau}+\varepsilon\rho_g\mathbf{g}+\mathbf{s}_p+\mathbf{s}_{\mathrm{ibm}}, \tag{6}$$

where ε is the local gas voidage (gas volume fraction), ρ_g the gas phase density, $\mathbf{u}$ the gas velocity, p the gas pressure, τ the viscous stress tensor, $\mathbf{g}$ the gravitational acceleration, $\mathbf{s}_{\mathrm{ibm}}$ the source term for the momentum exchange with large bodies such as an intruder, and $\mathbf{s}_p$ a source term which describes the momentum exchange with the small solid particles:

$$\mathbf{s}_p=\sum_{a=1}^{N_{\mathrm{part}}}\mathbf{F}_{\mathrm{d},a}\delta(\mathbf{r}-\mathbf{r}_a) \tag{7}$$

where the summation is performed over all particles and the drag force $\mathbf{F}_{\mathrm{d},a}$ is identical to what is used in the equation of motion of the particles. For the momentum exchange with small solid particles which are smaller than the Eulerian grid, it is necessary to introduce empirical drag correlations to take the gas–particle interaction into account:

$$\mathbf{F}_{\mathrm{d},a}=6\pi\mu_g R_a(\mathbf{u}-\mathbf{v}_a)\cdot\mathrm{F}(\mathrm{Re},\varepsilon) \tag{8}$$

where μ_g is the dynamic gas viscosity. For $F(\mathrm{Re},\varepsilon)$ the Ergun (1952) and Wen and Yu (1966) correlations are used:

$$F(\mathrm{Re},\varepsilon)=\begin{cases}\varepsilon^{-2.65}(1+0.15\,\mathrm{Re}^{0.687}) & \text{for } \varepsilon>0.8\\ \dfrac{150}{18}\dfrac{1-\varepsilon}{\varepsilon}+\dfrac{1.75}{18}\dfrac{\mathrm{Re}}{\varepsilon} & \text{for } \varepsilon<0.8\end{cases} \tag{9}$$

here $\mathrm{Re}=2R_a\rho_g\varepsilon|\mathbf{u}-\mathbf{v}_a|/\mu_g$ is the particle Reynolds number.

Details of the numerical implementation for the gas phase equations can be found in Van der Hoef et al. (2006) and Deen et al. (2007). Note that no turbulence modelling is taken into account since the turbulence is completely suppressed in the particle bed due to the high volume fraction of the solids particles (Van der Hoef et al., 2006).

2.3. Immersed boundary method

The interaction of the gas phase with an intruder larger than the size of the CFD cells is modelled with the immersed boundary method (IBM) where Lagrangian marker points are situated on the boundary of the large particle. Each marker exerts a force on the gas phase such that the local velocity of the gas is equal to the velocity of that marker. IBM has been widely used to study fluid-structure interaction and was pioneered by Peskin to investigate cardiac flow problems (Peskin, 2002). Subsequently, the method has been extended to flow around rigid bodies. The implementation that we adopt is along the lines of Uhlmann (2005). The IBM source term $\mathbf{s}_{\mathrm{ibm}}$ at the grid cell faces is calculated by summing the

contribution of all Lagrangian force points:

$$\mathbf{s}_{\mathrm{ibm}} = \sum_{m=1}^{N_{\mathrm{langr}}} \mathbf{F}_m \delta(\mathbf{r}-\mathbf{r}_m), \tag{10}$$

where in our discretised simulations $\mathbf{F}_m$ is constructed such that the forcing results in a zero slip velocity at the surface of the sphere and $\delta(\mathbf{r}-\mathbf{r}_m)$ is a volume weighing delta function which distributes the forces to the surrounding grid cell faces. For a detailed implementation of this method we refer to Deen et al. (2004), Gerner (2009), and Kriebitzsch (2011).

3. Simulation settings

In the simulation, we use a container with dimensions $6 \times 6 \times 12$ cm^3 (width, depth, height). It contains one large intruder and 2,000,000 granular particles. The intruder has a diameter of 1 cm, while the granular particles are of average diameter 0.5 mm, with a Gaussian size distribution ($\sigma = 0.02$ mm) to avoid excessive ordering of the bed. According to the experimental results shown in Nelson et al. (2008) and Seguin et al. (2008), the ratio between the size of the container and the intruder in our simulation ($L_{box}/d = 6$) is large enough so that the surrounding walls have no effect on the dynamics of the intruder. A schematic representation of the bed geometry is shown in Fig. 1. We choose the mesh size (for solving the gas phase equations) is equal to 2 mm. This ratio of 5 between the intruder diameter and the mesh size is sufficient to predict the drag forces with an error of less than 7% (Deen et al., 2012). Note that the mesh size cannot be reduced much further at the given granular particle size because of limitations imposed by the DPM approach, which dictates that the ratio between the mesh size the granular particle diameter should be at least 3 (Deen et al., 2007). A summary of all simulation parameters is given in Table 1.

In all simulations the coefficient of restitution is set to 0.97 for the normal direction, and to 0.33 for the tangential direction. For the particle–wall interaction the same collision parameters are used as for the particle–particle interaction. The friction coefficient is set to 0.1. All these values are typical for glass spheres/walls. We note that the normal spring stiffness k_n is in principle related to Young's modulus and the Poisson ratio of the solid material; however, in practice its value must be chosen much smaller to prevent the use of impractically small integration time steps. Therefore, the spring stiffness is chosen as low as possible while ensuring that the lowered spring stiffness does not have a significant influence on the phenomena observed. We investigated the influence of varying the spring stiffness between $k_n = 100$, 200, 400 and 800 N/m with an intruder initially located at $z = 0.11$ m and the initial velocity equal to 200 cm/s. The results showed that the lower normal stiffnesses do not significantly influence the collision kinematics (not shown). Thus, to enhance the computational efficiency, $k_n = 100$ N/m was used in all subsequent simulations. The granular particles are fluidized by a uniform upflow gas, which was gradually turned off such as to make the bed homogeneous with a flat surface. The depth of the static bed is about 6.34 cm with a solid fraction of about 0.62. Then we let the intruder fall downwards from some position above the bed. In the current simulations, the intruder with the highest downward velocity only penetrated half of the total granular depth.

Our simulations are very much inspired by the experimental work by Katsuragi and Durian (2007). However, a full one-to-one comparison is not possible due to the limitation of the computing capacity. That is, our granular particle size is about two times larger while the intruder is 2.5 times smaller than the experimental ones.

Table 1
Parameters used in the simulations.

Gravity z-direction	m/s^2	9.81
Intruder diameter	m	0.01
Intruder density	kg/m^3	2500
Particle diameter	m	5×10^{-4}
Particle density	kg/m^3	2500
Restitution coefficient (normal)	–	0.97
Restitution coefficient (tangential)	–	0.33
Friction coefficient	–	0.10
Normal spring stiffness	N/m	100
Tangential spring stiffness	N/m	32.13
Contact time step	s	7.2×10^{-5}
Gas viscosity	kg/(m s)	1.8×10^{-5}
Computation domain		
x-Direction	m	0.06
y-Direction	m	0.06
z-Direction	m	0.12
Number of grid cells		
x-Direction	–	30
y-Direction	–	30
z-Direction	–	60

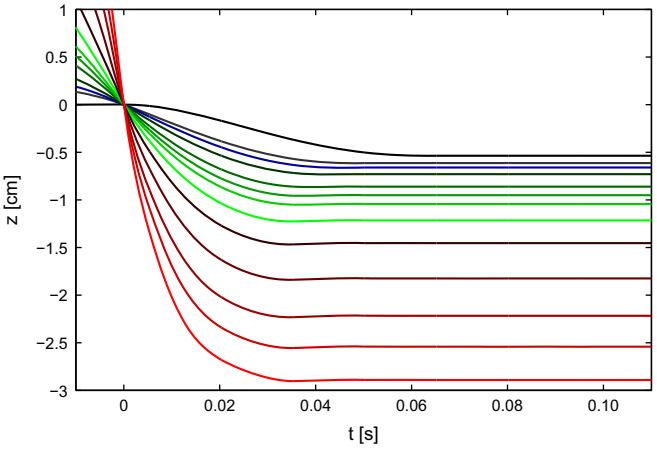

Fig. 2. Kinematics of impact for a glass intruder dropped onto a bed of glass beads: intruder depth, $z(t)$ versus time t. Curves are colour coded according to the initial impact speed of the intruder: $v_0 = 0$, −18, −24, −32, −46, −56, −66, −86, −116, −170, −242, −312, −404 cm/s, respectively, from black to red. (For interpretation of the references to colour in this figure caption, the reader is referred to the web version of this article.)

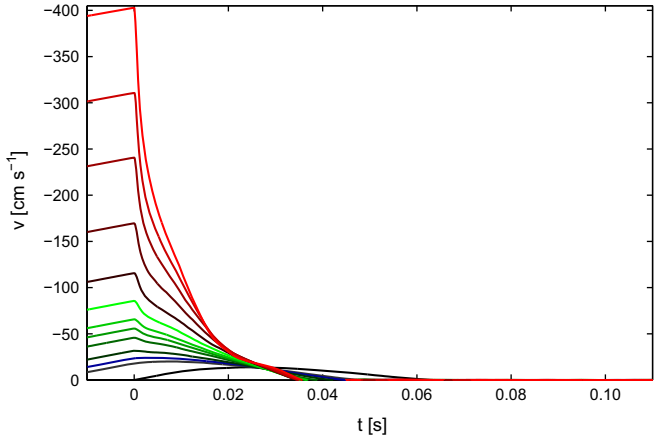

Fig. 3. Kinematics of impact for a glass sphere dropped onto a bed of glass beads: intruder speed, $v(t)$ versus time t. For colour coding, see Fig. 2.

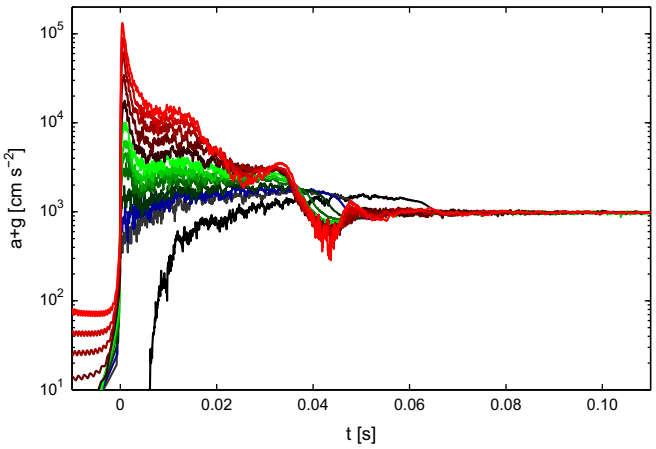

Fig. 4. Kinematics of impact for a glass sphere dropped onto a bed of glass beads: net acceleration, $a(t)+g$ versus time t. For colour coding, see Fig. 2.

4. Results and discussion

The complete data set of the position $z(t)$, velocity $v(t)$, and acceleration $a(t)+g$ of the intruder is shown in Figs. 2, 3 and 4, respectively. The time origin is *defined* as the time of initial impact, and the position is measured upwards from the granular surface, opposite to the gravity direction. The curves are colour-coded according to the initial impact speed of the intruder, v_0, which ranges from 0 to 400 cm/s, similar to the values used by Katsuragi and Durian (2007). The time evolution of the intruder dynamics is in qualitative good agreement with the experimental results, which are repeated here in Fig. 5 for clarity. We note that a quantitative agreement is not expected because due to computational limitations, our granular particle size is about two times larger while the intruder is 2.5 times smaller than the experimental one.

In Katsuragi and Durian (2007) it is stressed that, although the final position is approached smoothly, the velocity vanished abruptly with a discontinuity in acceleration. Similarly, in the work of Goldman and Umbanhowar (2008) two jumps of the force were observed during the impact: "a rapid, velocity dependent increase upon initial contact and a similarly sharp depth-dependent decrease as the impacting object comes to rest". Our simulations reproduce all these features, as is especially apparent from Fig. 5.

One of quantities that has been studied intensively is the stopping time. From our results, it is difficult to assess when the intruder is completely still. It may also be difficult to record this time in experiments, because obviously the rod or thread attached behind the intruder may influence the results and cannot show all details. In our simulations, the penetration time is defined as the first time the intruder velocity crosses 0 cm/s. The stopping time is plotted against the initial impact velocity, v_0 in Fig. 6. Just as in Pica Ciamarra et al. (2004) for a 4.46-cm diameter steel cylinder dropped sideways onto a bed of 0.46–0.64 cm diameter rods, the stopping time t_{stop} seems constant for fast impacts; however, in Katsuragi and Durian (2007) it is shown that this is only the limiting behaviour as t_{stop} increases for lower impact velocities. Our simulation result in Fig. 6 confirms this behaviour. Note that our values are larger than their data, which may be partially caused by the different means of measurement.

Many previous studies (Walsh and de Bruyn, 2004; Ambroso et al., 2005a; Katsuragi and Durian, 2007) have shown the dependence of the penetration depth d on the initial impact velocity, v_0. Our simulation results show the same trend, which is shown in Fig. 7.

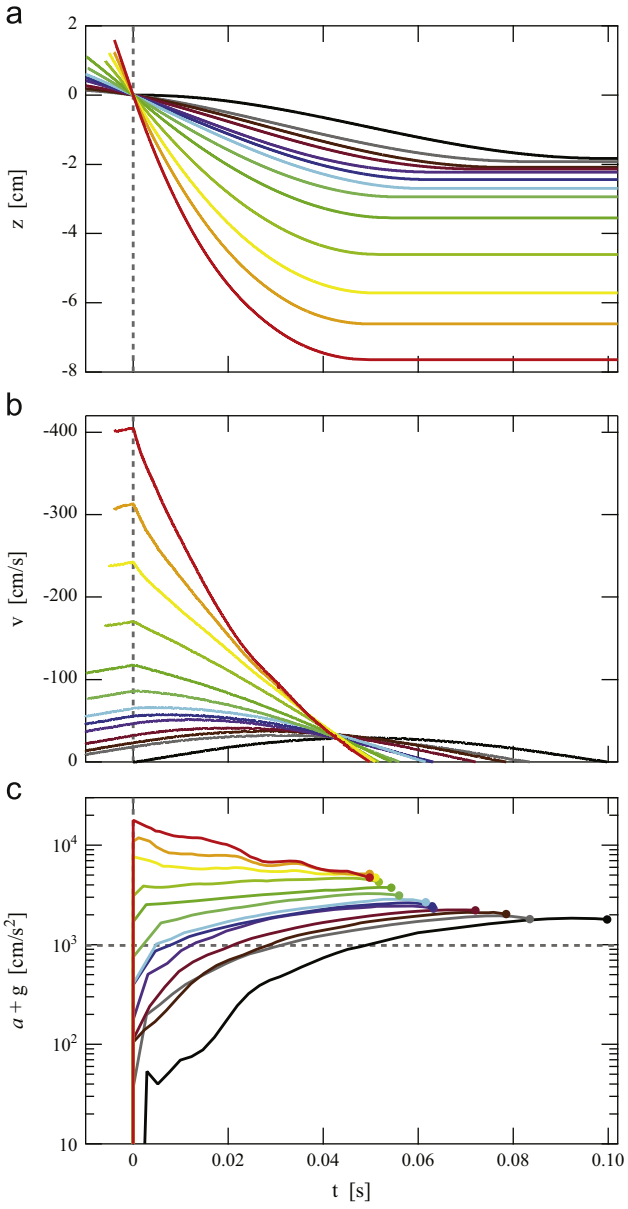

Fig. 5. Literature results for the intruder depth, speed and net acceleration versus time. Adapted by permission from Macmillan Publishers Ltd: Nature Physics (Katsuragi and Durian, 2007), copyright (2007). Note that the granular particle size is about two times smaller and the intruder 2.5 times larger than in our simulations.

In the final stage of the collision and before the settlement of the intruder, we can find that the intruder oscillated as if it were in contact with an elastic like medium. Both Katsuragi and Durian (2007) and Goldman and Umbanhowar (2008) observed oscillations in the movement of an intruder at the end of the collision. Katsuragi and Durian attributed this to the flexing of the brass mesh sieve located at the bottom of the container. Later, Goldman et al. excluded this effect. In our simulations both the intruder and the granular particles have the same physical properties, the intruder velocities become a critical parameter. As shown in Fig. 8, we find that by increasing the intruder impact velocity, the amplitude of the position oscillations increases.

All of the results shown above agree well with the existing experimental results, especially with the work in Katsuragi and Durian (2007). An advantage of a simulation method is the ability to show the gas effect on the intruder directly. Fig. 9 shows the ratio between gas–solid forces and contact forces on the large

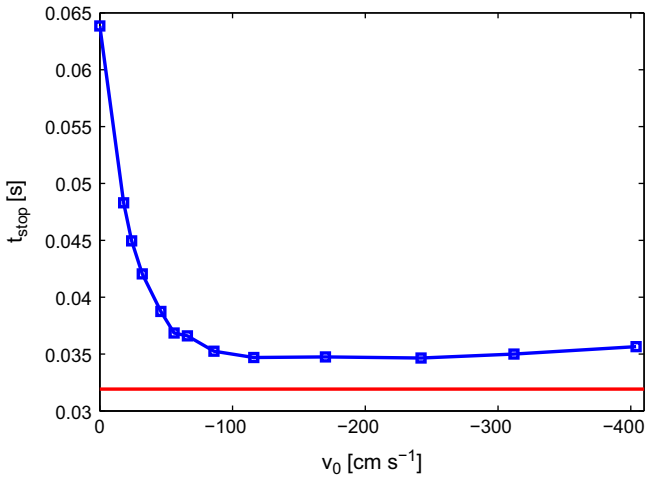

Fig. 6. Stopping time for different impact velocities. The red line is the characteristic time set by intruder size and gravity from the model described in Katsuragi and Durian (2007). (For interpretation of the references to colour in this figure caption, the reader is referred to the web version of this article.)

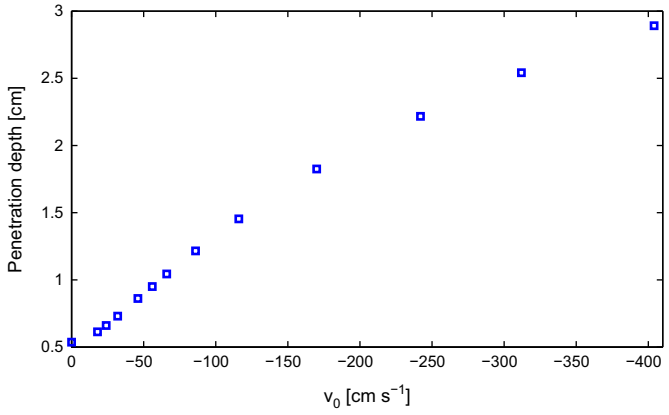

Fig. 7. Scaling behaviour of the absolute final penetration depth versus initial impact speed.

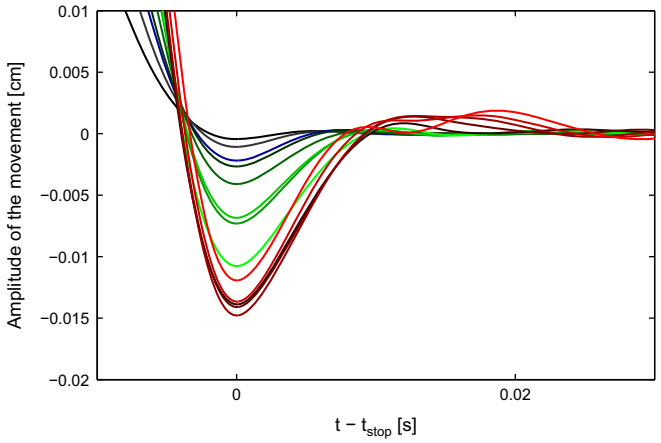

Fig. 8. At the end of the collision, the intruder rebounds and oscillates as if it were in contact with an elastic-like medium. For colour coding, see Fig. 2.

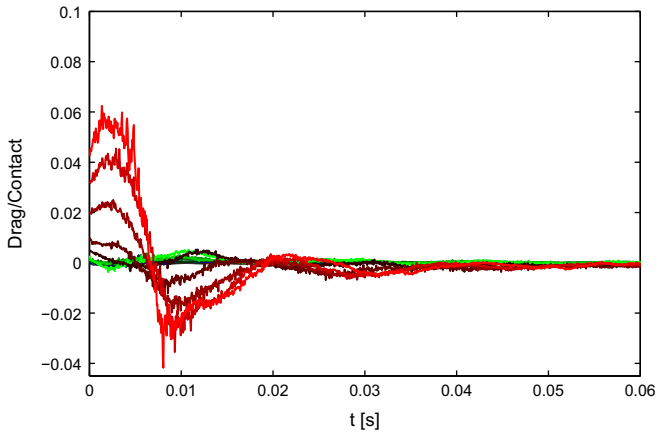

Fig. 9. The direct effect of gas: ratio of gas-induced forces to contact forces on the intruder. For colour coding, see Fig. 2.

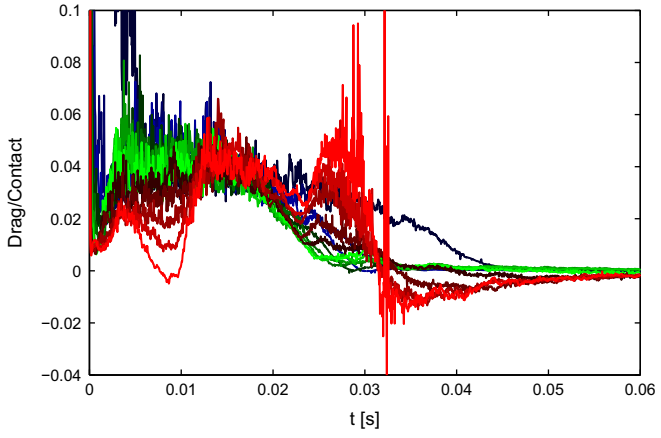

Fig. 10. The direct effect of gas of a two times smaller system: ratio of gas-induced forces to contact forces on the intruder. For colour coding, see Fig. 2.

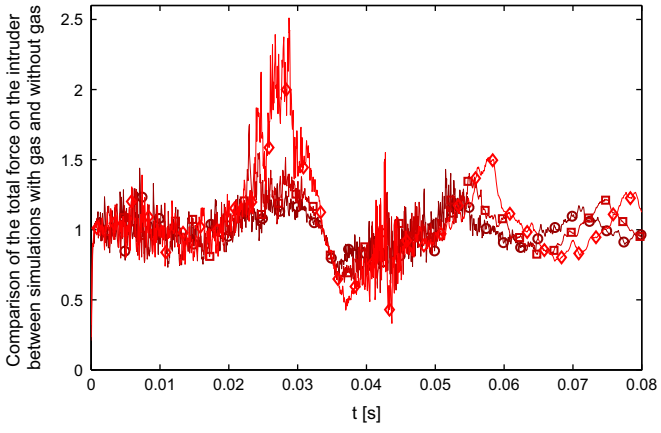

Fig. 11. The comparison of the total force on the intruder between different simulations with gas inside and without gas for $v_0 = -242$ (○), -312 (□), -404 (⋄) cm/s.

intruder. In Ambroso et al. (2005b) it is argued that the effect of the interstitial air is negligible. For the particular size of the granular particles (0.5 mm diameter) and intruder (1 cm diameter) shown here, our simulation results indicate that the direct gas drag on the intruder is relatively small, but not negligible, up to 5% of the total force on the intruder. As the size of the granular particles decreases, the interstitial gas may play an increasingly important role. To verify this, a two times smaller system of the granular particles (0.25 mm diameter) and intruder (0.5 cm diameter) was investigated. The results are shown in Fig. 10. The terminal velocities of the intruder in these simulations are the same as in the former case. The figure shows that the gas effect is even more pronounced, also at lower impact velocities, which is a

direct evidence that the kinematics of the granular particles is influenced by the drag they experience with the interstitial gas. Finally, to study the full gas effect we have performed additional simulations in which all gas effects have been disabled. These simulations show that the effect of interstitial air is very important, even for the relatively large (0.5 mm diameter) granular particles studied here. Fig. 11 shows the ratio of the total force experienced by the intruder with gas and without gas for $v_0 = -242$ cm/s $v_0 = -312$ cm/s $v_0 = 404$ cm/s. This ratio is observed to deviate substantially from 1, ranging from 0.5 and >2 for the higher impact velocities.

5. Conclusion

The goal of this paper was to introduce a state-of-the-art discrete particle method (DPM) combined with an immersed boundary (IB) method, which can be applied to study hydrodynamic effects of internal objects of any shape moving through a (pre-)fluidized granular bed. In this paper we focussed on the kinematics of a spherical intruder dropping onto a prefluidized granular bed of Geldart B particles, but may also be applied to other intruder shapes and smaller particles (as long as an appropriate contact model can be defined). We have shown that, overall, our simulation results are in good agreement with the existing experimental observations. The simulations offer a powerful tool to investigate the gas-induced and contact forces directly and independently. We have shown that the direct gas-induced force experienced by an intruder is small, but not negligible, for relatively large granular particles of 0.5 mm diameter and an intruder of 1 cm diameter. We have also shown that for smaller granular particles (0.25 mm diameter), the relative effect of the gas has grown significantly. In a forthcoming paper we will investigate these effects for even smaller granular particles, where even larger gas effects are expected, and for intruders dragged at constant velocity through the granular bed.

Acknowledgements

This work is part of the research program of the Foundation for Fundamental Research on Matter (FOM), which is part of the Netherlands Organization for Scientific Research (NWO).

References

Alder, B., Wainwright, T., 1957. Phase transition for a hard sphere system. Journal of Chemical Physics 27 (5), 1208–1209.
Ambroso, M., Kamien, R., Durian, D., 2005a. Dynamics of shallow impact cratering. Physical Review E 72 (4), 041305.
Ambroso, M.A., Santore, C.R., Abate, A.R., Durian, D.J., 2005b. Penetration depth for shallow impact cratering. Physical Review E 71, 051305.
Caballero, G., Bergmann, R., van der Meer, D., Prosperetti, A., Lohse, D., 2007. Role of air in granular jet formation. Physical Review Letters 99 (1), 018001.
Cundall, P.A., Strack, O.D., 1979. A discrete numerical model for granular assemblies. Geotechnique 29 (1), 47–65.
Deen, N.G., van Sint Annaland, M., Kuipers, J., 2004. Multi-scale modeling of dispersed gas–liquid two-phase flow. Chemical Engineering Science 59 (8), 1853–1861.
Deen, N., Van Sint Annaland, M., Van der Hoef, M., Kuipers, J., 2007. Review of discrete particle modeling of fluidized beds. Chemical Engineering Science 62 (1), 28–44.
Deen, N.G., Kriebitzsch, S.H., van der Hoef, M.A., Kuipers, J., 2012. Direct numerical simulation of flow and heat transfer in dense fluid-particle systems. Chemical Engineering Science 81, 329–344.
Ergun, S., 1952. Fluid flow through packed columns. Chemical Engineering Progress 48, 89–94.
Gerner, H.J., 2009. Newton vs Stokes: Competing Forces in Granular Matter. University of Twente.
Goldman, D., Umbanhowar, P., 2008. Scaling and dynamics of sphere and disk impact into granular media. Physical Review E 77 (2), 021308.
Katsuragi, H., Durian, D., 2007. Unified force law for granular impact cratering. Nature Physics 3 (6), 420–423.
Kondic, L., Fang, X., Losert, W., O'Hern, C.S., Behringer, R.P., 2012. Microstructure evolution during impact on granular matter. Physical Review E 85, 011305.
Kriebitzsch, S.H., 2011. Direct Numerical Simulation of Dense Gas–Solid Flows. Eindhoven University of Technology.
Lohse, D., Rauhé, R., Bergmann, R., van der Meer, D., 2004. Granular physics: creating a dry variety of quicksand. Nature 432 (7018), 689–690.
Nelson, E.L., Katsuragi, H., Mayor, P., Durian, D.J., 2008. Projectile interactions in granular impact cratering. Physical Review Letters 101, 068001.
Peskin, C.S., 2002. The immersed boundary method. Acta Numerica 11 (0), 479–517.
Pica Ciamarra, M., Lara, A., Lee, A., Goldman, D., Vishik, I., Swinney, H., 2004. Dynamics of drag and force distributions for projectile impact in a granular medium. Physical Review Letters 92 (19), 194301.
Royer, J., Corwin, E., Eng, P., Jaeger, H., 2007. Gas-mediated impact dynamics in fine-grained granular materials. Physical Review Letters 99 (3), 38003.
Royer, J.R., Corwin, E.I., Conyers, B., Flior, A., Rivers, M.L., Eng, P.J., Jaeger, H.M., 2008. Birth and growth of a granular jet. Physical Review E 78 (1), 011305.
Royer, J.R., Conyers, B., Corwin, E.I., Eng, P.J., Jaeger, H.M., 2011. The role of interstitial gas in determining the impact response of granular beds. Europhysics Letters 93 (2), 28008.
Seguin, A., Bertho, Y., Gondret, P., 2008. Influence of confinement on granular penetration by impact. Physical Review E 78, 010301.
Stukowski, A., 2009. Visualization and analysis of atomistic simulation data with OVITO—the open visualization tool. Modelling and Simulation in Materials Science and Engineering 18 (1), 015012.
Thoroddsen, S., Shen, A.Q., 2001. Granular jets. Physics of Fluids 13, 4.
Uehara, J., Ambroso, M., Ojha, R., Durian, D., 2003. Low-speed impact craters in loose granular media. Physical Review Letters 90 (19), 194301.
Uhlmann, M., 2005. An immersed boundary method with direct forcing for the simulation of particulate flows. Journal of Computational Physics 209 (2), 448–476.
Van der Hoef, M., Ye, M., van Sint Annaland, M., Andrews, A., Sundaresan, S., Kuipers, J., 2006. Multiscale modeling of gas-fluidized beds. Advances in Chemical Engineering 31, 65–149.
van Sint Annaland, M., Deen, N., Kuipers, J., 2005. Numerical simulation of gas–liquid–solid flows using a combined front tracking and discrete particle method. Chemical Engineering Science 60 (22), 6188–6198.
Wada, K., Senshu, H., Matsui, T., 2006. Numerical simulation of impact cratering on granular material. Icarus 180 (2), 528–545.
Walsh, A., de Bruyn, J., 2004. Penetration of spheres into loose granular media. Canadian Journal of Physics 82 (6), 439–446.
Wang, D., Ye, X., Zheng, X., 2012. The scaling and dynamics of a projectile obliquely impacting a granular medium. European Physical Journal E 35, 1–12.
Wen, C., Yu, Y., 1966. Mechanics of fluidization. In: Chemical Engineering Progress Symposium Series, vol. 62, p. 100.
Xiong, Q., Li, B., Zhou, G., Fang, X., Xu, J., Wang, J., He, X., Wang, X., Wang, L., Ge, W., Li, J., 2012. Large-scale DNS of gas-solid flow on Mole-8.5. Chemical Engineering Science 71, 422–430.